



**HAL**  
open science

## Pulsed reactive chemical vapor deposition in the C-Ti-Si system from H<sub>2</sub>/TiCl<sub>4</sub>/SiCl<sub>4</sub>

Sylvain Jacques, H. Di-Murro, M.-P. Berthet, H. Vincent

► **To cite this version:**

Sylvain Jacques, H. Di-Murro, M.-P. Berthet, H. Vincent. Pulsed reactive chemical vapor deposition in the C-Ti-Si system from H<sub>2</sub>/TiCl<sub>4</sub>/SiCl<sub>4</sub>. *Thin Solid Films*, 2005, 478 (1-2), pp.13-20. 10.1016/j.tsf.2004.09.043 . hal-03988790

**HAL Id: hal-03988790**

**<https://hal.science/hal-03988790>**

Submitted on 14 Feb 2023

**HAL** is a multi-disciplinary open access archive for the deposit and dissemination of scientific research documents, whether they are published or not. The documents may come from teaching and research institutions in France or abroad, or from public or private research centers.

L'archive ouverte pluridisciplinaire **HAL**, est destinée au dépôt et à la diffusion de documents scientifiques de niveau recherche, publiés ou non, émanant des établissements d'enseignement et de recherche français ou étrangers, des laboratoires publics ou privés.

## **Pulsed reactive chemical vapor deposition in the C-Ti-Si system from H<sub>2</sub>/TiCl<sub>4</sub>/SiCl<sub>4</sub>**

**S. JACQUES, H. DI-MURRO, M.-P. BERTHET and H. VINCENT**

Laboratoire des Multimatériaux et Interfaces —UMR 5615 CNRS / University of Lyon 1

43, boulevard du 11 Novembre 1918, Bâtiment Berthollet

F – 69622 Villeurbanne Cedex, France

### **Abstract,**

A new route was explored to produce Ti<sub>3</sub>SiC<sub>2</sub>-based thin coatings on carbonaceous substrates. This method combines low pressure-pulsed chemical vapor deposition (CVD) and reactive CVD, the gaseous phase being a mixture of SiCl<sub>4</sub>, TiCl<sub>4</sub> and H<sub>2</sub>. It consists in depositing a pyrocarbon film on the substrate, converting C into SiC (or TiC<sub>x</sub>) and then converting this carbide into Ti<sub>3</sub>SiC<sub>2</sub>. Experiments and thermodynamic calculations were performed and compared. The films were investigated by X-ray diffraction and transmission electron microscopy. Several microstructures consisting of various combinations of Ti<sub>3</sub>SiC<sub>2</sub>, C, SiC, TiC<sub>x</sub> and TiSi<sub>2</sub> were obtained.

**Keywords:** Chemical vapour deposition (CVD) (68), Carbides (57), Multilayers (299), Transmission electron microscopy (TEM) (496)

### **Corresponding author:**

Sylvain JACQUES,

Tel.: +33 472431392 ; Fax: +33 472440618

E-mail address: [sylvain.jacques@adm.univ-lyon1.fr](mailto:sylvain.jacques@adm.univ-lyon1.fr)

## 1. Introduction

Some of the useful properties of ceramics include high melting temperature, low density, high strength, wear resistance, and corrosion resistance. But contrary to many metals, ceramics have one major drawback: they are brittle. Some particular ceramic based materials, however, can overcome this problem. Titanium carbide-silicide  $Ti_3SiC_2$  is thus regarded to as promising material for a number of applications in severe conditions. It combines the advantage of both metals and ceramics, it is soft and easily machinable, behaves plastically and maintains its strength at high temperature [1] and it is moreover stable to at least  $1300^{\circ}C$  [2]. The high plasticity of  $Ti_3SiC_2$  is explained by its layered structure with double  $Ti_6C$  blocks separated by a square-planar Si sheet; the interaction between  $Ti_6C$  and Si atom being weak [3]. Furthermore  $Ti_3SiC_2$  has a high resistance to crack formation (fracture toughness:  $7.20 \text{ MPa m}^{1/2}$ ), a low hardness of about 4 GPa, it is a damage-tolerant material. Grain pull out, grain delamination and crack deflection are the main mechanisms that enhance its fracture toughness [4].  $Ti_3SiC_2$  coatings could be deposited by chemical vapor deposition (CVD) from different gas mixtures such as  $TiCl_4$ - $SiCl_4$ - $CCl_4$ - $H_2$  [5-7] or  $TiCl_4$ - $SiCl_4$ - $CH_4$ - $H_2$  [8]. These studies highlighted in particular that the deposition of pure  $Ti_3SiC_2$  is difficult and when the ternary compound is processed by CVD, the weakly bonded basal planes are oriented perpendicular to the substrate surface.

On the other hand, a good toughness can be also achieved with ceramic composites by adding between the fiber and the matrix a sub-micrometer thin layered film called "interphase" that governs the debond and sliding resistance of the fiber/matrix interface [9].

Naslain *et al.* [10] have demonstrated that a nano-scale multilayered interphase (PyC/SiC)<sub>n</sub> composed of n alternations of pyrocarbon (PyC) and carbide sub-layers prepared by low pressure-pulsed CVD (P-CVD) can fulfil this purpose. The P-CVD method allows to control accurately the residence time, the maturation of the gas phase and to obtain a thickness of films as low as a few nanometers. Lackey *et al.* have shown that it is also possible to obtain laminated matrix composed of alternate layers of PyC and SiC using the forced-flow-thermal-gradient CVI process [11]. Such a laminated matrix may also contribute to mechanical toughness. In a more recent study carried out in our laboratory, (PyC/TiC)<sub>n</sub>, multilayered interphases were prepared within SiC/SiC minicomposites by pressure-pulsed reactive CVD (P-RCVD): a new method that combines P-CVD with reactive CVD. In the interphase, each carbon layer is deposited from propane and each TiC layer is obtained from the TiCl<sub>4</sub>-H<sub>2</sub> gaseous phase in which only the titanium element is present, the carbon element being supplied by the previously deposited carbon layer [12,13]. Compared with pure pyrocarbon interphase, the lifetime of minicomposites with (PyC/TiC)<sub>n</sub> interphases at 700°C in air under load were improved. It might be interesting to extend this study by adding SiCl<sub>4</sub> to the precursor gas for carbide layer deposition. Hence, it might be possible to process (i) double TiC-SiC layers as in reference [14] in alternation with PyC layers or perhaps (ii) thin layers of Ti<sub>3</sub>SiC<sub>2</sub> if the conditions of the gas phase are well controlled. In the last case owing to its layered structure, the ternary carbide phase itself may play the role of a mechanical fuse. In both cases, we can expect to obtained composites with further improved composite lifetime owing to the protective effect of SiO<sub>2</sub> formed during oxidation in addition to TiO<sub>2</sub> [4].

The aim of this present work was first to attempt to synthesize pure Ti<sub>3</sub>SiC<sub>2</sub> by P-RCVD. But in case of co-deposition with other carbide phases, the formation of a nano-scale multilayered coating thanks to the pulsed method could be also interesting. The principle

relies on a sequence of short time reactions between a solid reactive substrate (C, SiC or TiC<sub>x</sub>) and a SiCl<sub>4</sub>-TiCl<sub>4</sub>-H<sub>2</sub> gas mixture. The deposition was studied as a function of the composition of the solid substrate and of the input gas phase, so two reactive systems were explored: SiC(s)-TiCl<sub>4</sub>(g)-H<sub>2</sub>(g) and TiC<sub>x</sub>(s)-SiCl<sub>4</sub>(g)-H<sub>2</sub>(g). The choice of processing conditions was facilitated by a thermodynamic evaluation of the systems at equilibrium. Film microstructures, determined by X-ray diffraction (XRD) and transmission electron microscopy (TEM) were closely correlated with processing conditions.

## 2. Thermodynamic analysis

A thermodynamic analysis was made to examine situations involving P-RCVD conversion of carbonaceous compounds into Ti<sub>3</sub>SiC<sub>2</sub>. The calculation has been planned according to the free-energy minimization method. The computer program (Gemini 2) and the thermodynamic data come from the Scientific Group Thermodata Europ (Saint Martin d'Hères, France).

This program allows calculations on non-stoichiometric compounds such as TiC<sub>x</sub> and Ti<sub>5</sub>Si<sub>3</sub>C<sub>y</sub> in the ranges  $0.58 \leq x \leq 0.97$  and  $0 \leq y < 1$  using the generalized multisublattice model. A total of 14 solids and 63 gases were considered (Tab. 1). The temperature was 1100°C which is a maximum for our reactor chamber made of quartz. The total pressure was set as low as 5 kPa in order to favor coating homogeneity.

First, the ternary phase diagram of Ti-Si-C was calculated (Fig. 1). This isothermal section is very similar to those previously presented in the literature and obtained either from experimental results or from computation [15-18]. This similarity demonstrates that the used thermodynamic data are reliable. At this temperature, it emerges that the ternary phase

$\text{Ti}_3\text{SiC}_2$  is in equilibrium with SiC,  $\text{TiSi}_2$  and the phases  $\text{TiC}_x$  and  $\text{Ti}_5\text{Si}_3\text{C}_y$  with high carbon contents ( $0.725 \leq x < 0.97$  and  $y = 0.96$ ).

### *2.1 Reaction of $\text{H}_{2(g)}/\text{TiCl}_{4(g)}$ gaseous mixture on SiC*

The RCVD diagram shown in Fig. 2 displays the predicted solid phases present at equilibrium according to the initial SiC-TiCl<sub>4</sub>-H<sub>2</sub> composition. The three dotted lines drawn in the triangle from the SiC vertex correspond to three hydrogen to reactant dilution ratios R (0.5, 1.5 and 6.7). It comes out that the compound  $\text{Ti}_3\text{SiC}_2$  cannot be obtained with  $R < 0.5$ . For  $R > 0.5$ , the action of  $\text{H}_2/\text{TiCl}_4$  on SiC can result in  $\text{Ti}_3\text{SiC}_2$  (T1) formation over a wide range of composition. This ternary phase T1 co-exists with  $\text{TiC}_x$ , SiC and even with the solid solution  $\text{Ti}_5\text{Si}_3\text{C}_x$  (T2) for  $R > 6.7$ . However, a narrow single-phase  $\text{Ti}_3\text{SiC}_2$  region is predicted in this diagram if SiC reacts with a very large excess of gaseous reagent.

The difficulty for RCVD modelling comes from the knowledge of the exact initial system composition. If the experimental control of the initial gas composition (i.e. the value of the dilution ratio R, which is regulated by means of mass flow controllers) is direct and immediate, the control of the gas quantity actually in contact with the initial solid substrate is complex. This quantity depends not only on diffusion phenomena, but also on the progress of the initiation growth step and then on the thickness of the new growing solid layer. As and when the substrate is coated with a new solid scale, it is gradually separated from the gas; this feature decreases the initial substrate to gas quantity ratio. In practice for the computation, the gas quantity was gradually increased while maintaining a constant initial substrate quantity (i.e. one mole of SiC). The evolution of the solid phase compositions is presented following this method in Fig. 3. Such charts allow a precise visualization of the conditions for single-

phase  $\text{Ti}_3\text{SiC}_2$  deposition. As a general rule, with a large excess of  $\text{TiCl}_4$  ( $> 10^5$  mol), it is possible to consume the whole SiC substrate without depositing the faintest solid coating. With a large excess of  $\text{TiCl}_4$  ( $> 10^4$  mol) the final solid phase is only  $\text{TiC}_x$ . With  $R < 6.7$ , SiC can be converted to pure solid  $\text{Ti}_3\text{SiC}_2$  (and gases) if the initial quantity of  $\text{TiCl}_4$  is thoroughly monitored; however the single-phase  $\text{Ti}_3\text{SiC}_2$  deposition domain is broader with  $R = 4$  ( $4 < \text{TiCl}_4/\text{SiC} < 2000$ ) than with  $R = 1.5$  ( $10 < \text{TiCl}_4/\text{SiC} < 100$ ). For  $R > 6.7$ , Fig. 3.c confirms that  $\text{Ti}_3\text{SiC}_2$  can be co-deposited with  $\text{Ti}_5\text{Si}_3\text{C}_x$ .

## 2.2 Reaction of $\text{H}_{2(g)}/\text{SiCl}_{4(g)}$ gaseous mixture on $\text{TiC}_x$

The initial substrate is a  $\text{TiC}_x$  film previously deposited from a RCVD reaction between a carbon substrate and  $\text{H}_2$ - $\text{TiCl}_4$  gaseous phase. In that case, the composition of this carbide depends particularly on the coating thickness. A  $\text{TiC}_{0.967}$  carbide can be expected if the film is very thin ( $\ll 1 \mu\text{m}$ ) or else a sub-stoichiometric  $\text{TiC}_x$  ( $0.58 < x < 0.967$ ) [19,20]. So, in order to estimate the influence of  $\text{TiC}_x$  substrate composition on  $\text{Ti}_3\text{SiC}_2$  deposition, two  $x$  values were considered for the thermodynamic calculation: 0.967 and the intermediate value 0.7.

Isothermal sections showing the solid phases obtained at equilibrium are presented in Fig. 4 for  $\text{TiC}_x$ - $\text{SiCl}_4$ - $\text{H}_2$  systems. With both  $x = 0.967$  and  $x = 0.7$  values there is no single-phase  $\text{Ti}_3\text{SiC}_2$  deposition domain. The  $\text{TiC}_x$  substrate is either partly or totally turned into  $\text{Ti}_3\text{SiC}_2$  mixed with SiC or with SiC and  $\text{TiSi}_2$ .

Fig. 5 shows the quantity evolution of produced solid species as a function of the gaseous reagent quantity reacting with one mole of  $\text{TiC}_x$ . These charts confirm that for  $\text{Ti}_3\text{SiC}_2$  co-deposition the initial system composition must be well monitored

( $0.1 < \text{SiCl}_4/\text{TiC}_x < 10$ ). The conversion yield of  $\text{TiC}_x$  into  $\text{Ti}_3\text{SiC}_2$  is maximum for an initial  $\text{SiCl}_4/\text{TiC}_x$  ratio equal to 1. Above this ratio, thermodynamics forecast the formation of  $\text{SiC}$  and  $\text{TiSi}_2$  (in small quantity with  $R = 4$ ) and even of free silicon when a high hydrogen content is used in the gaseous mixture. These results are similar if a  $\text{TiC}_{0.7}$  substrate is considered instead of a  $\text{TiC}_{0.967}$  substrate (Fig. 5.c).

### 3. Experimental procedure.

The thermodynamic study tends to show that obtaining pure  $\text{Ti}_3\text{SiC}_2$  is difficult and requires a very strict control of the gaseous phase quantity introduced within the reactor and actually reacting with the previously deposited layer. A pressure-pulsed reactive CVD (P-RCVD) method should allow such control: for example, by simply varying the number of gas pulses, it is possible to obtain a nucleation of isolated grain islands or the growth of nano-scale carbide layers [12,13]. This method combines P-CVD with RCVD. Pulsed methods are based on a succession of phased cycles (called “pulses”) [10,21,22]. The three phases of one pulse are:

- introduction of gas mixture in the reactor chamber during 0.5 s and thus increase of reactor pressure,
- reaction of gases with the substrate or with the previously deposited sub-layer during three seconds in the closed reactor,
- evacuation phase fixed to 4.5 seconds.

The P-RCVD apparatus included a horizontal quartz tube (30 mm in inner diameter) heated by an electrical resistor furnace. The temperature was  $1100^\circ\text{C}$  within a 10 cm in length

quasi-isothermal hot area. The gaseous species were fed to the reactor and evacuated through pneumatic valves operated with an automatic control device. A rotary vane vacuum pump was used at the outlet of the apparatus and equipped with liquid nitrogen traps. Buffer tanks (fed through mass flow controllers) were placed upstream from the furnace in order to have sufficient gas supplies at disposal for rapid peak pressure establishment within the reactor chamber. The CVD apparatus, the status statement of the valves during pulse sequences as well as an example of pressure variation versus time are schematically represented in Fig. 6.

In each case, a pyrocarbon (PyC) sub-layer was previously deposited from propane (with a supply pressure of 2.5 kPa) in order to be used as a new carbon source for further carbide formation. Then, the  $H_2/MCl_4$  gaseous mixtures (M is Ti or Si) were introduced in the reactor with an operating pressure set at 5 kPa and a dilution ratio R equal to 4 as recommended by the thermodynamic study.

In the case of P-RCVD in the  $TiC_{x(s)}-SiCl_{4(g)}-H_{2(g)}$  system, a repetitive pulse sequence was designated as  $(P_p/T_t/S_s)_n$  where p was the number of propane pulses chosen for each previously deposited PyC sub-layer, t the number of  $H_2/TiCl_4$  pulses chosen for each  $TiC_x$  sub-layer formation, s the number of  $H_2/SiCl_4$  (which reacts with  $TiC_x$ ) pulses and n the total number of repeated sequences. The example of a pressure cycling given in Fig. 6.c corresponds to one  $(P_3/T_2/S_1)_1$  sequence. For P-RCVD in the  $SiC_{(s)}-TiCl_{4(g)}-H_{2(g)}$  system, the sequences were  $(P_p/S_s/T_t)_n$ .

The different coatings were deposited both on polycrystalline graphite disks (10 mm in diameter, Ellor 30 from Carbone Lorraine France) and on SiC Hi-Nicalon fibers (from Nippon Carbon, Japan). The coatings deposited on graphite disks were characterized by X-ray

diffraction (XRD: Philips PW 3710,  $\lambda_{\text{Cu}} = 0,15418$  nm). The coatings deposited on Hi-Nicalon fibers (14  $\mu\text{m}$  in diameter) were characterized by TEM: (TOPCON 002B, Japan) using bright-field (BF), high resolution and selected-area electron diffraction (SAED) techniques. This microscope was equipped with a Kevex energy dispersive spectroscopy (EDS) equipment for chemical analysis. Only titanium and silicon were considered in the coating analysis (not carbon). The thin sheets for TEM examination were prepared by following the method described elsewhere [23].

## 4. Results and discussion.

### 4.1 P-RCVD in the $\text{TiC}_{x(s)}\text{-SiCl}_{4(g)}\text{-H}_{2(g)}$ system

A first coating has been processed using the following sequence: (P<sub>800</sub>/T<sub>600</sub>/S<sub>600</sub>)<sub>1</sub>. The carbide film which has grown on the PyC layer is 1  $\mu\text{m}$  thick. Despite a poor signal-to-noise ratio due to the low coating thickness, the XRD pattern revealed two peaks located at 34.2° and 39.6° which were assigned respectively to  $\text{Ti}_3\text{SiC}_2$  {101} and {104} (Fig. 7). TEM observation has revealed that the coating is made of carbide crystal grains with stacking faults and having a size ranging from 50 nm to more than 200 nm. A part of these carbide grains was identified with cubic SiC or other polytypes like 6H-SiC (Fig. 8.a). In that case, EDS analysis has confirmed titanium absence. Another part was identified with  $\text{Ti}_3\text{SiC}_2$  crystals without preferred orientation (Fig. 8.b and 9). The three titanium to one silicon ratio was confirmed by EDS analysis. Finally, a few crystals containing both titanium and silicon could not be faithfully identified but could correspond to  $\text{TiSi}_2$  as forecast by thermodynamics (Fig. 5.a). According to a preliminary study and Rapaud's work [12] carried out in the Ti-C system by using the same P-RCVD reactor, the 600 H<sub>2</sub>/TiCl<sub>4</sub> pulses on PyC should have led to the growth of a 0.5-1  $\mu\text{m}$  thick  $\text{TiC}_x$  layer. But here, no area without silicon was detected,

which indicates that the whole  $\text{TiC}_x$  initially deposited from  $\text{TiCl}_4$  has been converted into silicon-containing carbides during P-RCVD with  $\text{SiCl}_4$ . Thus, according to the thermodynamic study, the sequence  $(\text{P}_{800}/\text{T}_{600}/\text{S}_{600})_1$  allows to have a  $\text{SiCl}_4/\text{TiCl}_4$  ratio above one and therefore to co-deposit the ternary phase  $\text{Ti}_3\text{SiC}_2$  with especially SiC (Fig. 5.a).

A second coating was deposited using graded sequences:  $(\text{P}_{20}/\text{T}_{15}/\text{S}_s)_{16}$  with  $s$  increasing from 0 to 15 (in unit steps from one sequence to the other). With 15  $\text{H}_2/\text{TiCl}_4$  pulses, the initial  $\text{TiC}_x$  sub-layers are continuous and have a thickness of a few nanometers [12,13]. Unlike RCVD micrometer thick  $\text{TiC}_x$  films, the titanium carbide is expected to be nearly stoichiometric in that case. For this coating, the ternary phase  $\text{Ti}_3\text{SiC}_2$  was not detected by XRD. Only the  $\{111\}$   $\text{TiC}_x$  and/or SiC peak could be distinguished on the XRD pattern. TEM analysis specifies the nature of the coating (Fig. 10). The BF image allows the 16 sub-layers, which appears well separated, to be counted. The SAED pattern showed, in addition to the TiC/SiC spots, the turbostratic pyrocarbon  $\{002\}$  arcs indicating that PyC was not totally consumed during carbide RCVD growth and remains intercalated between carbide sub-layers. By selecting the four last carbide sub-layers with an objective aperture diaphragm, the EDS analysis showed in this area the presence of Ti and Si in the ratio 3:2. Hence, the various observations only revealed the presence of nano-crystallised TiC and SiC grains mixture. The  $\text{H}_2/\text{SiCl}_4$  gas mixture has therefore partially converted  $\text{TiC}_x$  into SiC without obtaining  $\text{Ti}_3\text{SiC}_2$ . Rapaud *et al.* have reported that, compared with pure pyrocarbon interphase and despite the poor oxidation resistance of  $\text{TiC}_x$ , the lifetimes of minicomposites with  $(\text{PyC}/\text{TiC})_n$  interphases at  $700^\circ\text{C}$  in air under load are improved [12,13]. The introduction of SiC within the  $\text{TiC}_x$  sub-layers of the nano-scale multilayered interphase should further increase its high temperature resistance.

#### 4.2 P-RCVD of SiC in the PyC<sub>(s)</sub>-SiCl<sub>4(g)</sub>-H<sub>2(g)</sub> system

Before using the conditions recommended by thermodynamics for single-phase Ti<sub>3</sub>SiC<sub>2</sub> deposition (i.e. RCVD in the SiC<sub>(s)</sub>-TiCl<sub>4(g)</sub>-H<sub>2(g)</sub> system), it was necessary to study first the growth of SiC from action of H<sub>2</sub>/SiCl<sub>4</sub> gaseous mixture on pyrocarbon. For this purpose, a graded multilayered coatings was processed using 22 sequences (P<sub>5</sub>/S<sub>s</sub>)<sub>22</sub> with s increasing from 10 to 73 (by step of 3 from one sequence to the other). From TEM observation, only the last 6-8 out of the 22 expected SiC sub-layers are observed (Fig. 11). This result indicates that at least about fifty H<sub>2</sub>/SiCl<sub>4</sub> pulses are necessary for the growth of a 10 nm thick continuous SiC layer whereas only fifteen H<sub>2</sub>/TiCl<sub>4</sub> pulses are enough for continuous TiC<sub>x</sub> sub-layer formation. While carbon can diffuse through non stoichiometric TiC<sub>x</sub>, its diffusion is stopped as soon as a stoichiometric SiC continuous film is formed preventing any further carbide growth. Thus, contrary to RCVD of TiC<sub>x</sub> where the growth of several micrometers thick carbide is possible, increasing the number of gas pulses does not allow thicker SiC films than a few nanometers to be obtained.

#### 4.3 P-RCVD in the SiC<sub>(s)</sub>-TiCl<sub>4(g)</sub>-H<sub>2(g)</sub> system

In this system, a first coating was processed using graded sequences (P<sub>20</sub>/S<sub>70</sub>/T<sub>t</sub>)<sub>10</sub> with t increasing from 10 to 100 (by step of 10 from one sequence to the other); the attack of the 10 nm thick SiC sub-layers was done by gradually increasing the number of H<sub>2</sub>/TiCl<sub>4</sub> pulses. In that case, the BF TEM image shows that the carbide sub-layers are partly welded together with the presence of local pores (Fig. 12). EDS analysis indicates that the coating contains only 2-5 at. % of Si. Furthermore, the {002} PyC arcs are not observed in the SAED pattern. Thus, both PyC and SiC were consumed during carbide growth and the coating is mainly

made of porous  $\text{TiC}_x$ . The high number of  $\text{H}_2/\text{TiCl}_4$  pulses on very thin PyC/SiC sub-layers associated with the great reactivity of  $\text{TiCl}_4$  can explain this result, which was actually forecasted by the thermodynamic calculations for high  $\text{TiCl}_4/\text{SiC}$  ratio (Fig. 3.b,  $5 \cdot 10^3 < \text{TiCl}_4/\text{SiC} < 10^5$ ).

For the last coating, the number of  $\text{H}_2/\text{TiCl}_4$  pulses was drastically reduced in order to prevent the total consumption of the previously deposited SiC sub-layers. The sequences were  $(\text{P}_{20}/\text{S}_{70}/\text{T}_t)_{10}$  with  $t$  increasing from 1 to 10 (in unit steps from one sequence to the other). This time, a nano-scale multilayered coating (PyC/SiC+ $\text{TiC}_x$ ) very similar to the one obtained with  $(\text{P}_{20}/\text{T}_{15}/\text{S}_s)$  sequences in paragraph 4.1 is observed by SAED and BF TEM. In that case, the silicon content measured by EDS ranged from 15 to 40 % at. The ternary phase  $\text{Ti}_3\text{SiC}_2$  was not detected. This result does not seem to be in agreement with thermodynamics, which forecasted the presence of either pure  $\text{Ti}_3\text{SiC}_2$  or pure  $\text{TiC}_x$  at equilibrium (Fig. 3.b). A too low  $\text{TiCl}_4/\text{SiC}$  ratio ( $< 0.1$ ) associated with an unfavorable kinetic of reaction could explain a partial conversion of SiC into  $\text{TiC}_x$ .

## 5. Conclusion.

This study has shown that, in accordance with the thermodynamic computation, it is possible to co-deposit by P-RCVD without preferred orientation the ternary phase  $\text{Ti}_3\text{SiC}_2$  with SiC in a micrometer thick film. This method also enables to process from  $\text{C}_3\text{H}_8$ ,  $\text{H}_2/\text{TiCl}_4$  and  $\text{H}_2/\text{SiCl}_4$  nano-scale multilayered coatings (PyC/ $\text{TiC}+\text{SiC}$ ) in which the carbide sub-layers are made of a nano-crystallised mixture of  $\text{TiC}_x$  and SiC grains.

But in the case of nano-scale coatings,  $\text{Ti}_3\text{SiC}_2$  is never obtained. Regardless of the number of gas pulses on thin carbide sub-layers, it seems impossible to reach the favorable

gas/solid ratio required by thermodynamics for  $\text{Ti}_3\text{SiC}_2$  deposition. In the  $\text{SiC}_{(s)}\text{-TiCl}_{4(g)}\text{-H}_{2(g)}$  system in which single phase  $\text{Ti}_3\text{SiC}_2$  formation is thermodynamically possible, the deposition of a micrometric thick SiC film before  $\text{H}_2/\text{TiCl}_4$  pulses should enable a better monitoring of the gas to solid ratio. Unfortunately, the growth of thick SiC films by P-RCVD from  $\text{SiCl}_4$  is unachievable at  $1100^\circ\text{C}$ . The use of methyltrichlorosilane  $\text{CH}_3\text{SiCl}_3$  and  $\text{H}_2$  for SiC growth by P-CVD [10] should make up for this limitation.

## References

- [1] M. W. Barsoum, T. El-Raghy, *J. Am. Ceram. Soc.* 79 (1996) 1953.
- [2] C. Racault, F. Langlais, R. Naslain, *J. Mater. Sci.* 29 (1994) 3384.
- [3] N. I. Medvedeva, D. L. Novikov, A. L. Ivanovski, M. V. Kuznetsov, A. J. Freeman, *Phys. Rev. B* 58 (1998) 16042.
- [4] S. Li, J. Xie, J. Zhao, L. Zhang, *Mater. Lett.*, 57 (2002) 119
- [5] J. J. Nickl, K. K. Schweitzer, P. Luxenberg, *J. Less Common Met.* 26 (1972) 335.
- [6] T. Goto, T. Hirai, *Mater. Res. Bull.* 22 (1987) 1195.
- [7] E. Pickering, W. J. Lackey, S. Crain, *Chem. Vap. Deposition* 6 (2000) 289.
- [8] C. Racault, F. Langlais, R. Naslain, Y. Kihn, *J. Mater. Sci.* 29 (1994) 3941.
- [9] A.G. Evans, D. Marshall, *Acta Metall* 37 (1989) 2567.
- [10] R. R. Naslain, R. Paillet, X. Bourrat, S. Bertrand, F. Heurtevent, P. Dupel, F. Lamouroux, *Solid State Ionics* 141-142 (2001) 541.
- [11] W. J. Lackey, S. Vaidyaraman, K. L. More, *J. Am. Ceram. Soc.* 80 (1997) 113.
- [12] O. Rapaud, Ph. D., Thesis n°169, University of Lyon1, France, 2002.
- [13] O. Rapaud, S. Jacques, H. Di-Murro, H. Vincent, M.-P. Berthet; J. Bouix, *J. Mater. Sci.* 39 (2004) 173-180.
- [14] H. Vincent, J.P. Scharff, C. Vincent, J. Bouix, *Mat. High Temp.* 10 (1992) 2.

- [15] M. Touanen, F. Teyssandier, M. Ducarroir, *J. Mater. Sci. Lett.* 8 (1989) 98.
- [16] W. J. J. Wakelkamp, F. J. J. van Loo, R. Metselaar, *J. Eur. Ceram. Soc.* 8 (1991) 135.
- [17] C. Racault, F. Langlais, C. Bernard, Part I, *J. Mater. Sci.* 29 (1994) 5023.
- [18] Y. Du, J. C. Schuster, H. J. Seifert, F. Aldinger, *J. Am. Ceram. Soc.* 83 (2000) 197.
- [19] C. Vincent, J. Dazord, H. Vincent, J. Bouix, *Thermochim. Acta* 138 (1989) 81 (in French).
- [20] O. Rapaud, H. Vincent, C. Vincent, S. Jacques, J. Bouix in: D. Davazoglou, C Vahlas (Eds.), *proc. 13th European Conference on Chemical Vapour Deposition (EUROCVD 13)*, Glifada, Athens, Greece, August 26-31, 2001, *J. Phys. IV, EDP Sciences, Les Ulis France*, 11 Pr3 (2001) p.391.
- [21] P. Dupel, R. Pailler, X. Bourrat, R. Naslain, *J. Mater. Sci.* 29 (1994) 1056.
- [22] P. Dupel, X. Bourrat, R. Pailler, *Carbon* 33 (1995) 1193.
- [23] S. Jacques, A. Guette, F. Langlais, X. Bourrat, *J. Mater. Sci.* 32 (1997) 2969.

### Table and Figure captions

Table 1. Species considered in the thermodynamic analysis.

Fig.1. Calculated 1100°C isothermal section of the Ti-Si-C diagram.

Fig.2. Calculated reactive deposition diagram for gaseous mixture  $H_2/TiCl_4$  action on SiC at 1100°C and 5 kPa (each symbol corresponds to one calculated result) (T1 is  $Ti_3SiC_2$ , T2 is  $Ti_5Si_3C_x$ ,  $R = H_2/TiCl_4$ ).

Fig.3. Calculated quantities of solid species produced at equilibrium from  $\{H_2/TiCl_4\}$  gaseous mixture reaction on 1 mole of SiC for  $R = 1.5$  (a)  $R = 4$  (b) and  $R = 8$  (c) versus the quantity of  $TiCl_4$  (T1 is  $Ti_3SiC_2$ , T2 is  $Ti_5Si_3C_x$ ,  $R = H_2/TiCl_4$ , 1100°C, 5 kPa).

Fig.4. Calculated reactive deposition diagram at 1100°C and 5 kPa for gaseous mixture  $\{H_2/SiCl_4\}$  action on  $TiC_{0.967}$  (a) and  $TiC_{0.7}$  (b) (each symbol corresponds to one calculated result) (T1:  $Ti_3SiC_2$ , T2:  $Ti_5Si_3C_x$ ,  $R = H_2/SiCl_4$ ).

Fig.5. Calculated quantities of solid species produced at equilibrium from  $\{H_2/SiCl_4\}$  gaseous mixture reaction on 1 mole of  $TiC_x$  for  $x = 0.967$  and  $R = 4$  (a),  $x = 0.967$  and  $R = 15$  (b) and  $x = 0.7$  and  $R = 15$  (c) versus the quantity of  $SiCl_4$  (T1:  $Ti_3SiC_2$ , 1100°C, 5 kPa).

Fig.6. Schematics of P-RCVD apparatus (a), valve states versus pulse CVD step (b), and example of a pulse sequence:  $(P_3/T_2/S_1)_1$  (c).

Fig.7. XRD pattern of  $(P_{800}/T_{600}/S_{600})_1$  coating.

Fig.8. SAED patterns of a 6H-SiC crystal taken along  $[73\bar{1}]$  zone axis (a) and of a  $Ti_3SiC_2$  crystal taken along  $[48\bar{1}]$  zone axis (b). The coating sequence was  $(P_{800}/T_{600}/S_{600})_1$ .

Fig.9. SAED pattern of a  $Ti_3SiC_2$  crystal taken along  $[010]$  zone axis (coating sequence:  $(P_{800}/T_{600}/S_{600})_1$ ). Insert: the distance between two spots corresponds to the c cell parameter of  $Ti_3SiC_2$  ( $d_{001}$ : 1.765 nm).

Fig.10. BF TEM observation and SAED pattern (insert) of the nano-scale  $(P_{20}/T_{15}/S_s)_{16}$  coating ( $s = \{0,1,2,\dots,15\}$ ).

Fig.11. SAED pattern (a), BF TEM (b) and high resolution TEM (c) observation of the nano-scale  $(P_5/S_s)_{22}$  coating ( $s = \{10,13,16,\dots,73\}$ ).

Fig.12. BF TEM observation and SAED pattern (insert) of the  $(P_{20}/S_{70}/T_t)_{10}$  coating ( $t = \{10,20,30,\dots,100\}$ ).

solid species	gaseous species
C, Si, Ti, SiC, TiC <sub>x</sub>	Si, Si <sub>2</sub> , Ti, C, C <sub>2</sub> , C <sub>3</sub> , H <sub>2</sub> , H, Cl <sub>2</sub> , Cl, HCl
TiSi <sub>2</sub> , TiSi, Ti <sub>5</sub> Si <sub>4</sub> , Ti <sub>5</sub> Si <sub>3</sub> , Ti <sub>3</sub> Si ; TiCl <sub>2</sub> ,	SiH, SiH <sub>2</sub> , SiH <sub>3</sub> , SiH <sub>4</sub> , Si <sub>2</sub> H <sub>6</sub>
TiH <sub>2</sub>	SiCl, SiCl <sub>2</sub> , SiCl <sub>3</sub> , SiCl <sub>4</sub> , Si <sub>2</sub> Cl <sub>6</sub>
Ti <sub>3</sub> SiC <sub>2</sub> (T1), Ti <sub>5</sub> Si <sub>3</sub> C <sub>y</sub> (T2)	TiCl, TiCl <sub>2</sub> , TiCl <sub>3</sub> , TiCl <sub>4</sub> , Ti <sub>2</sub> Cl <sub>6</sub>
	HSiCl, HSiCl <sub>3</sub> , H <sub>2</sub> Si <sub>2</sub> Cl <sub>2</sub> , SiH <sub>3</sub> Cl, SiH <sub>2</sub> Cl <sub>2</sub> , SiH <sub>4</sub>
	CH <sub>4</sub> , C <sub>2</sub> H <sub>2</sub> , C <sub>2</sub> H <sub>4</sub> , C <sub>2</sub> H <sub>6</sub> , CH <sub>2</sub> , CH <sub>3</sub>
	Si <sub>2</sub> , SiC, Si <sub>2</sub> C, Si <sub>3</sub> C, Si <sub>4</sub> C
	CCl, CCl <sub>2</sub> , C <sub>2</sub> Cl, CCl <sub>4</sub> , CHCl, CHCl <sub>2</sub> , CHCl <sub>3</sub> , C <sub>2</sub> HCl,
	C <sub>2</sub> HCl <sub>3</sub> , C <sub>2</sub> HCl <sub>4</sub> , C <sub>2</sub> HCl <sub>5</sub> , C <sub>2</sub> H <sub>2</sub> Cl <sub>2</sub> , C <sub>2</sub> H <sub>2</sub> Cl <sub>3</sub> , C <sub>2</sub> H <sub>2</sub> Cl <sub>4</sub> ,
	C <sub>2</sub> H <sub>3</sub> Cl, C <sub>2</sub> H <sub>4</sub> Cl <sub>2</sub> ,
	C <sub>2</sub> H <sub>8</sub> Si, ClHSi, ClH <sub>3</sub> Si, Cl <sub>2</sub> H <sub>3</sub> Si,

Table 1. Species considered in the thermodynamic analysis.

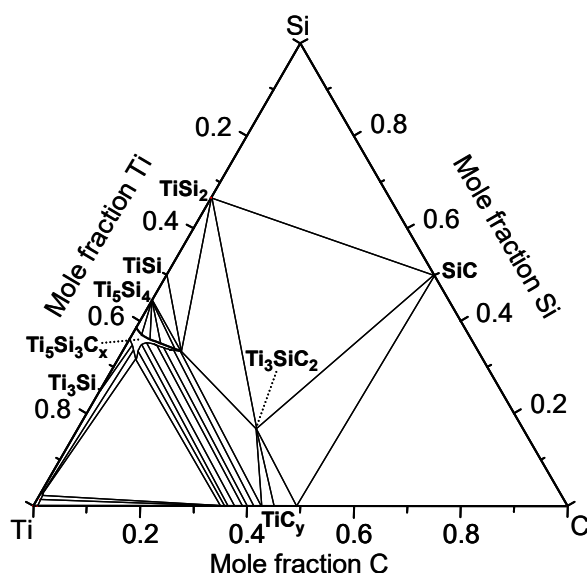


Fig. 1. Calculated 1100°C isothermal section of the Ti-Si-C diagram

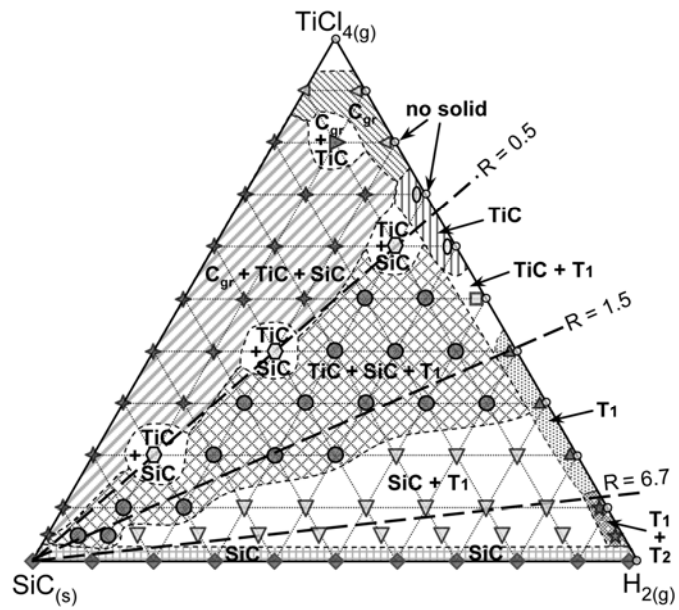


Fig. 2. Calculated reactive deposition diagram for gaseous mixture  $H_2/TiCl_4$  action on  $SiC$  at  $1100^\circ C$  and  $5\text{ kPa}$  (each symbol corresponds to one calculated result) ( $T_1$  is  $Ti_3SiC_2$ ,  $T_2$  is  $Ti_5Si_3C_x$ ,  $R = H_2/TiCl_4$ ).

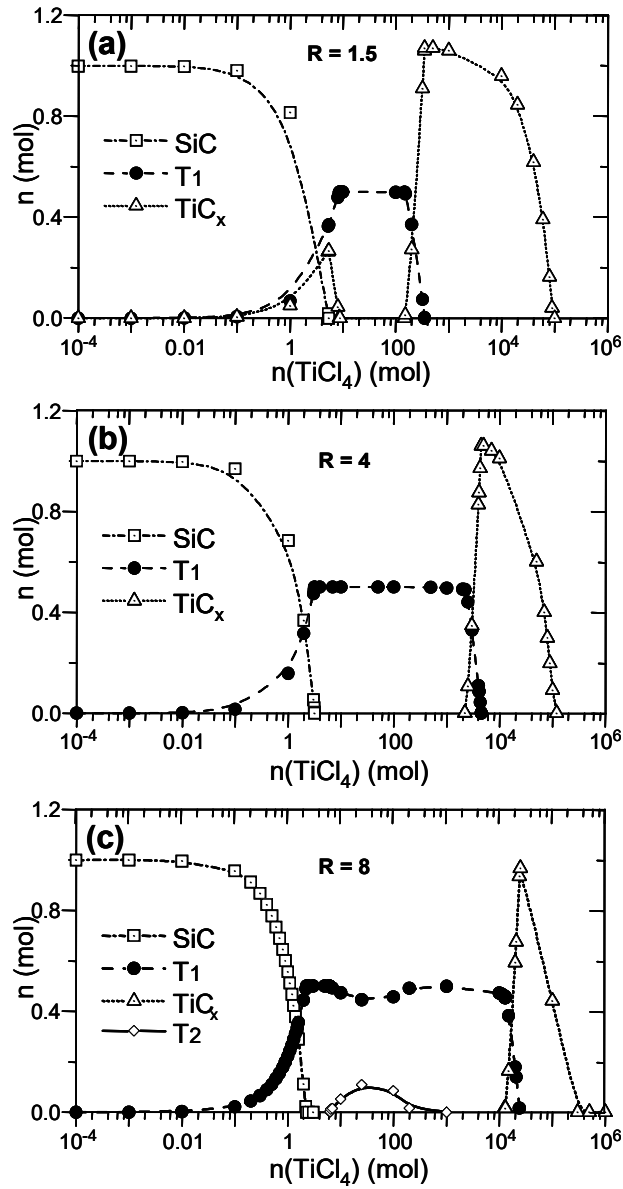


Fig. 3. Calculated quantities of solid species produced at equilibrium from  $\{H_2/TiCl_4\}$  gaseous mixture reaction on 1 mole of SiC for  $R = 1.5$  (a)  $R = 4$  (b) and  $R = 8$  (c) versus the quantity of  $TiCl_4$  (T1 is  $Ti_3SiC_2$ , T2 is  $Ti_5Si_3C_x$ ,  $R = H_2/TiCl_4$ ,  $1100^\circ C$ , 5 kPa).

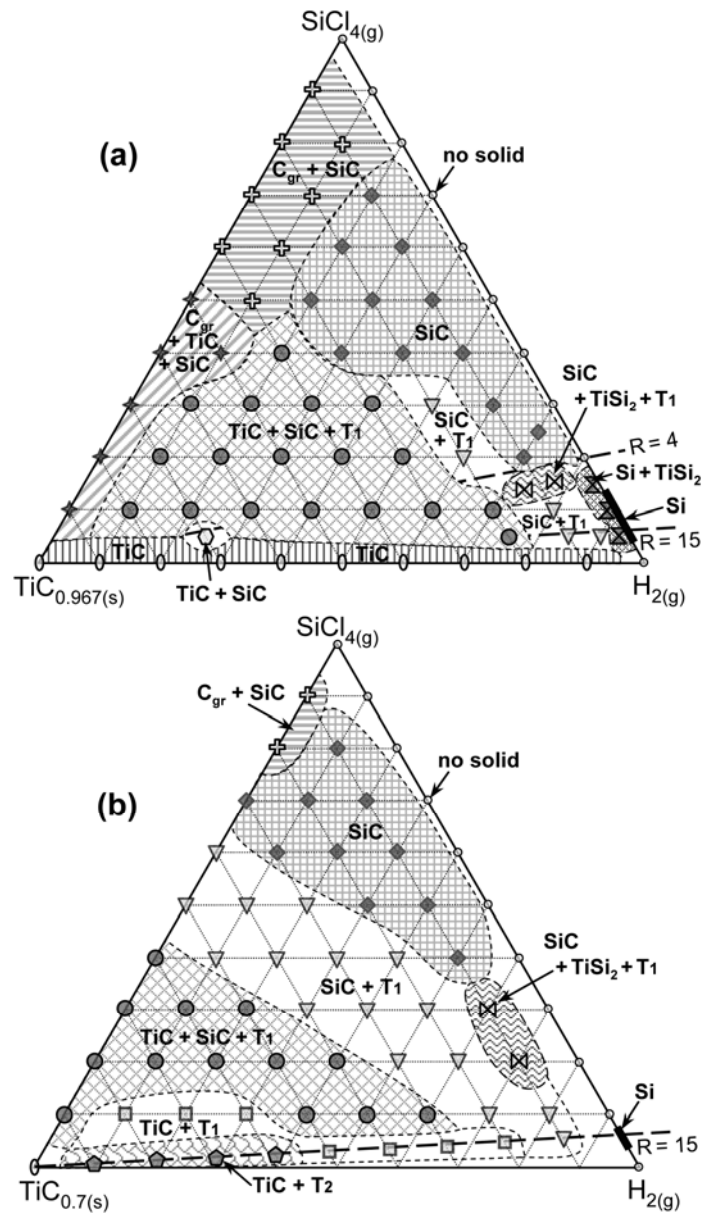


Fig. 4. Calculated reactive deposition diagram at 1100°C and 5 kPa for gaseous mixture  $\{\text{H}_2/\text{SiCl}_4\}$  action on  $\text{TiC}_{0.967}$  (a) and  $\text{TiC}_{0.7}$  (b) (each symbol corresponds to one calculated result) ( $\text{T}_1$ :  $\text{Ti}_3\text{SiC}_2$ ,  $\text{T}_2$ :  $\text{Ti}_5\text{Si}_3\text{C}_x$ ,  $R = \text{H}_2/\text{SiCl}_4$ ).

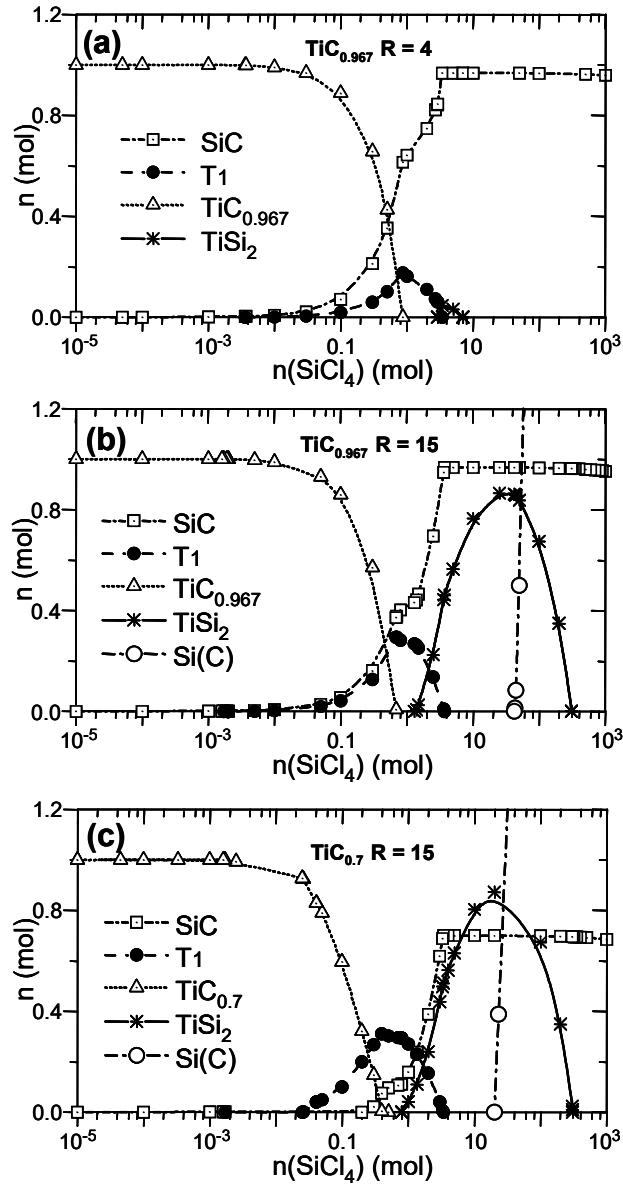


Fig. 5. Calculated quantities of solid species produced at equilibrium from  $\{\text{H}_2/\text{SiCl}_4\}$  gaseous mixture reaction on 1 mole of  $\text{TiC}_x$  for  $x = 0.967$  and  $R = 4$  (a),  $x = 0.967$  and  $R = 15$  (b) and  $x = 0.7$  and  $R = 15$  (c) versus the quantity of  $\text{SiCl}_4$  ( $\text{T1}$ :  $\text{Ti}_3\text{SiC}_2$ ,  $1100^\circ\text{C}$ ,  $5\text{ kPa}$ ).

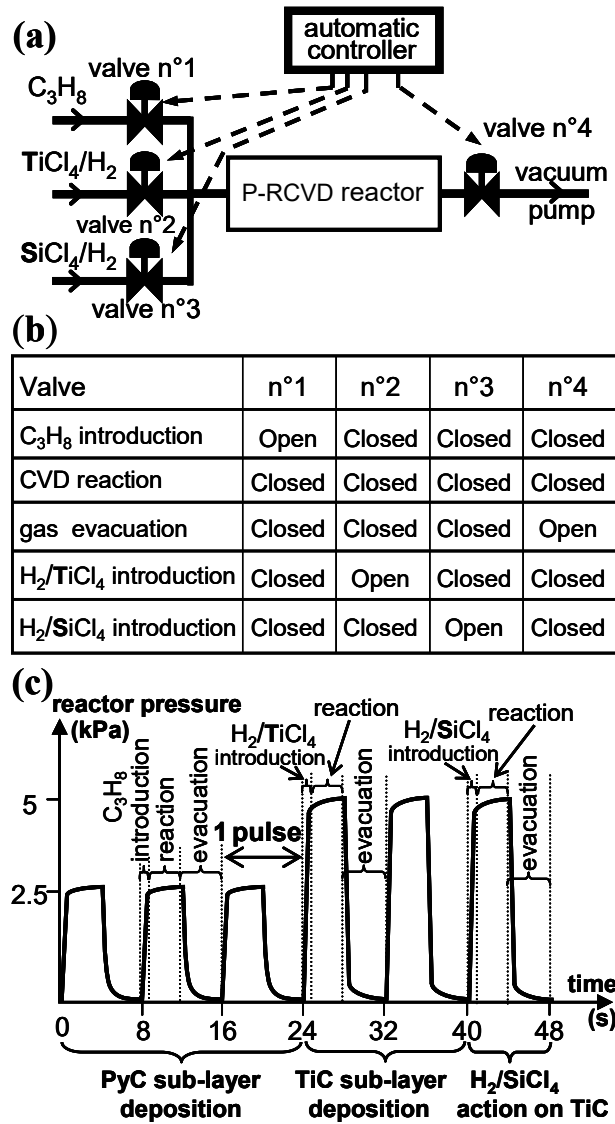


Fig. 6. Schematics of P-RCVD apparatus (a), valve states versus pulse CVD step (b), and example of a pulse sequence:  $(P_3/T_2/S_1)_1$  (c).

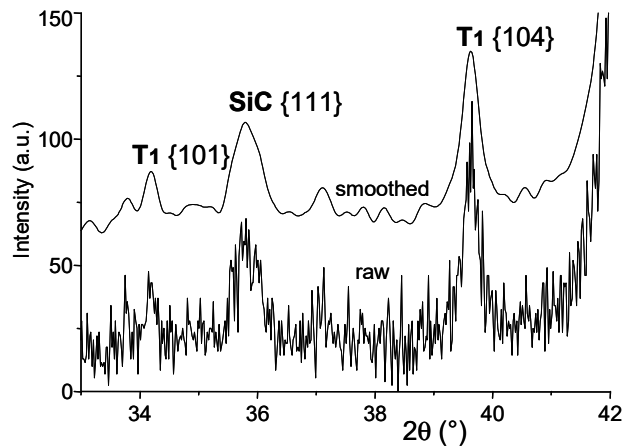


Fig. 7. XRD pattern of  $(P_{800}/T_{600}/S_{600})_1$  coating.

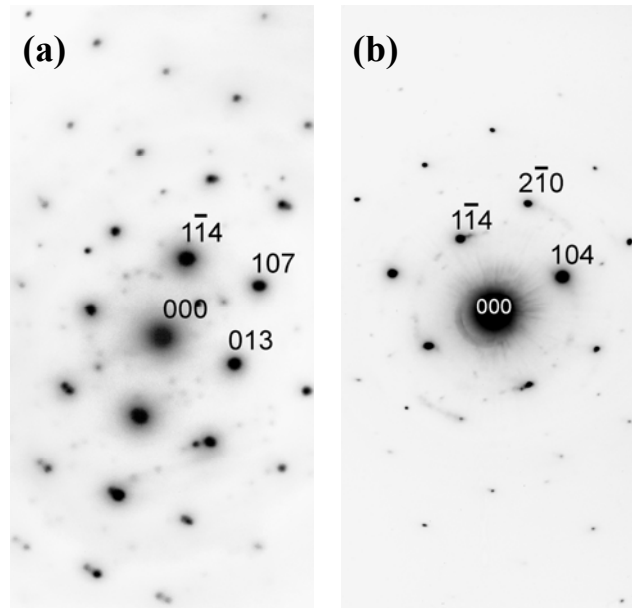


Fig. 8. SAED patterns of a 6H-SiC crystal taken along  $[73\bar{1}]$  zone axis (a) and of a  $\text{Ti}_3\text{SiC}_2$  crystal taken along  $[48\bar{1}]$  zone axis (b). The coating sequence was  $(\text{P}_{800}/\text{T}_{600}/\text{S}_{600})_1$ .

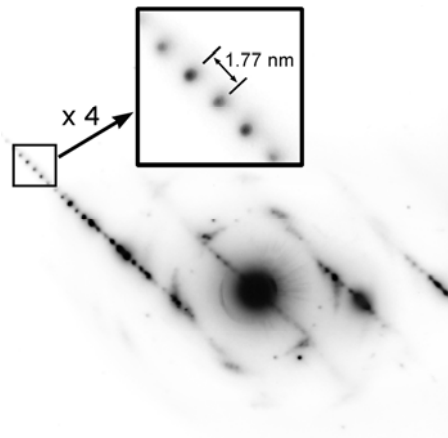


Fig. 9. SAED pattern of a  $\text{Ti}_3\text{SiC}_2$  crystal taken along  $[010]$  zone axis (coating sequence:  $(\text{P}_{800}/\text{T}_{600}/\text{S}_{600})_1$ ). Insert: the distance between two spots corresponds to the  $c$  cell parameter of  $\text{Ti}_3\text{SiC}_2$  ( $d_{001}$ : 1.765 nm).

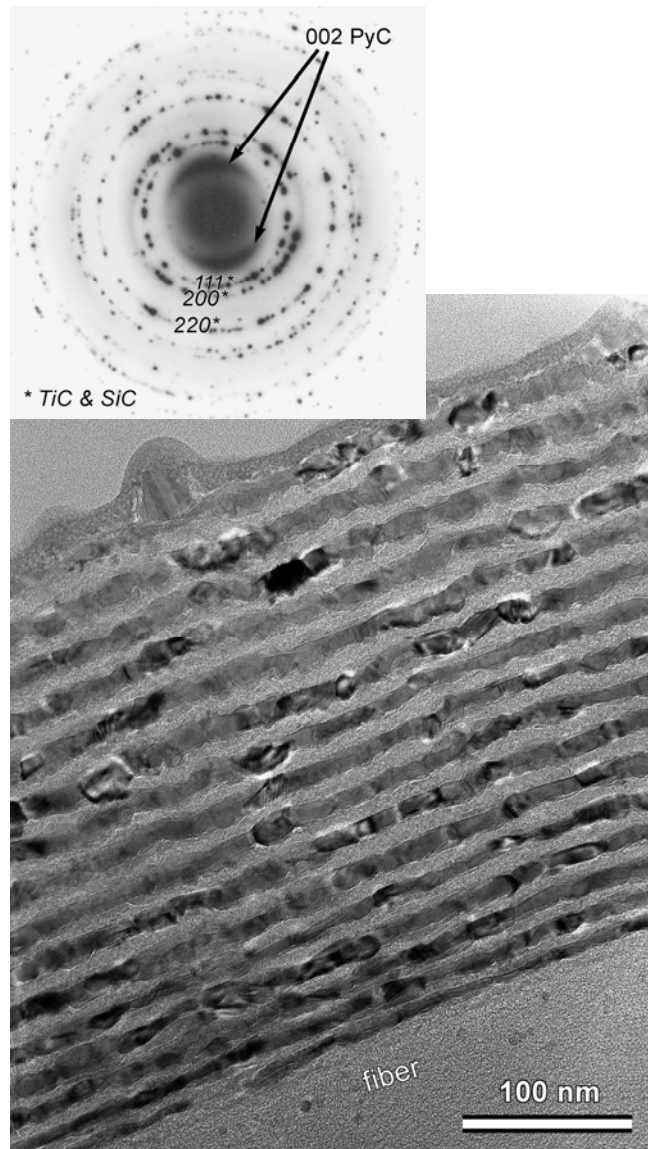


Fig. 10. BF TEM observation and SAED pattern (insert) of the nanoscale  $(P_{20}/T_{15}/S_s)_{16}$  coating ( $s = \{0,1,2,\dots,15\}$ ).

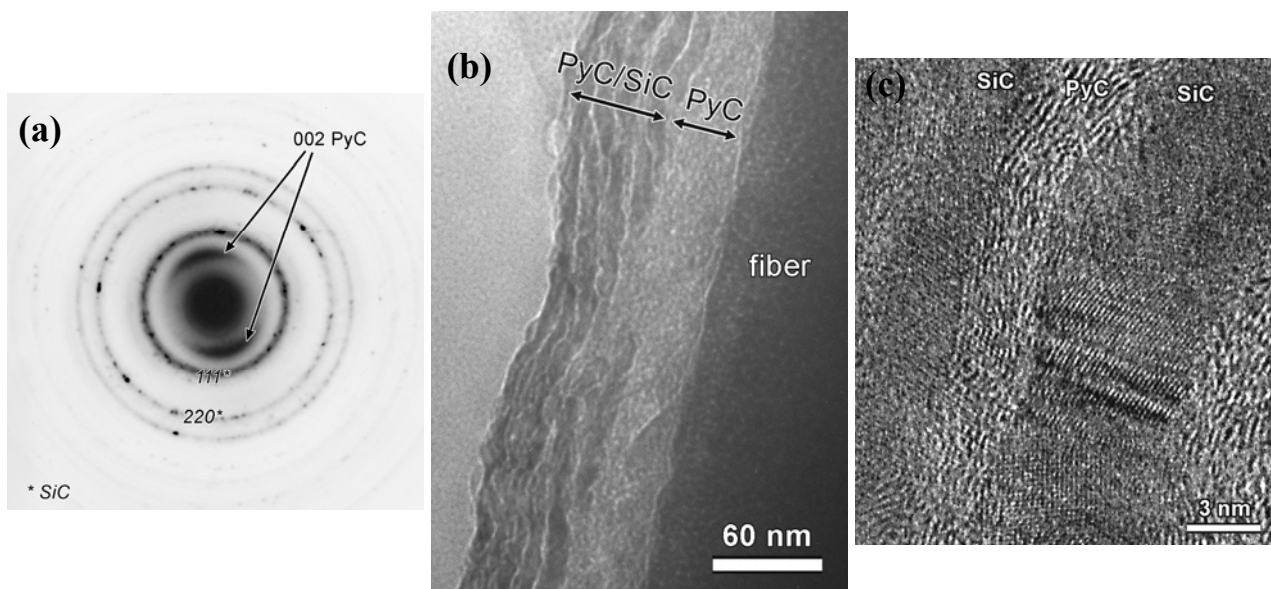


Fig. 11. SAED pattern (a), BF TEM (b) and high resolution TEM (c) observation of the nanoscale  $(P_5/S_s)_{22}$  coating ( $s = \{10,13,16,\dots,73\}$ ).

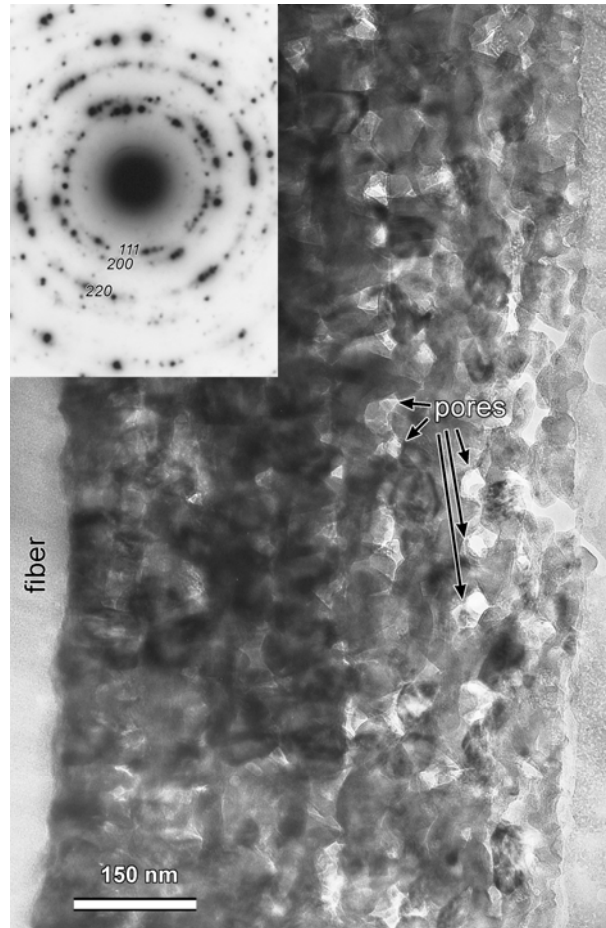


Fig. 12. BF TEM observation and SAED pattern (insert) of the  $(P_{20}/S_{70}/T_t)_{10}$  coating ( $t = \{10, 20, 30, \dots, 100\}$ ).